AIMS Mathematics, 9(6): 16704–16720.
DOI: 10.3934/math.2024810
Received: 19 January 2024
Revised: 16 March 2024
Accepted: 16 April 2024
Published: 14 May 2024

http://www.aimspress.com/journal/Math

Research article

An attention-based bidirectional long short-term memory based optimal deep learning technique for bone cancer detection and classifications

Thavavel Vaiyapuri[1,*], Prasanalakshmi Balaji[2], S. Shridevi[3], Santhi Muttipoll Dharmarajlu[4] and Nourah Ali AlAseem[5]

[1] College of Computer Engineering and Sciences, Prince Sattam Bin Abdulaziz University, Al Kharj, Saudi Arabia
[2] Department of Computer Science, College of Computer Science, King Khalid University, Abha, Saudi Arabia
[3] Centre for Advanced Data Science, Vellore Institute of Technology, Chennai
[4] College of Nursing, Jazan University, Jazan, Kingdom of Saudi Arabia
[5] College of Computer Engineering and Sciences, Prince Sattam Bin Abdulaziz University, Al Kharj, Saudi Arabia

* **Correspondence:** Email: t.thangam@psau.edu.sa.

Abstract: Bone cancer detection is an essential region of medical analysis but developments in medical imaging and artificial intelligence (AI) are vital. Using approaches, namely deep learning (DL) and machine learning (ML), radiologists and medical staff can examine X-ray, CT, and MRI scans to identify bone cancer and abnormalities. These technologies support earlier diagnosis, correct diagnosis, and treatment planning, enhancing patient solutions. The combination of AI-driven image analysis and the knowledge of medical practitioners improves the speed and precision of bone cancer detection, contributing to more effectual clinical activities. DL algorithms, particularly CNNs, are exposed to great performance in image classification tasks and are extremely utilized for medical image analysis. We offer a Hybrid Rice Optimization Algorithm with DL-Assisted Bone Cancer Detection (HROADL-BCD) technique on medical X-ray images. The major intention of the HROADL-BCD method is to examine the X-ray images for the recognition of bone cancer. In the presented HROADL-BCD method, a bilateral filtering (BF) process was performed to remove the noise. To derive feature vectors, the HROADL-BCD technique applied the EfficientNet model. The HROADL-BCD technique involved the HROA for hyperparameter tuning of the EfficientNet model. Last, the bone cancer detection and classification process were executed by the attention-based bidirectional long short-term memory

(ABiLSTM) approach. A wide range of simulations could be applied for the simulation result analysis of the HROADL-BCD algorithm. The extensive outcome of the HROADL-BCD approach inferred the superior outcome of 97.62% outcome concerning various aspects.

Keywords: medical imaging; bone cancer; computer-aided diagnosis; Rice Optimization Algorithm; deep learning
Mathematics Subject Classification: 94A60, 11T71, 68P25

1. Introduction

Bone cancer arises from strong cells and then initiates cancer. The initial sign of bone tumor is bone cancer. The cancer develops steadily and can extend to different body parts [1]. It can ruin the bone tissues and then make the bone fragile. According to the data, 3,500 persons in the USA were afflicted with bone cancer in 2018. Approximately 47 percent of people with bone cancer perish. Through many tests, the surgeon analyzes the tumors. The X-ray radiograph analysis is utilized to identify tumors in the bones of humanoids. The strong bone and the tumorous bone X-ray integration rates are dissimilar [2]. Because of that, a tumorous bone image surface seems shabby. The bone cancer harshness is dignified by a phase and the status. Tumor progress level is employed by physicians to forecast the illness progress ratio [3]. Analyzing tumors in the bone needs proficiency. A physician does bone cancer analyses physically; therefore, it is time-consuming, and there is a chance of a mistake.

Initial recognition appears to be the mere factor that enhances the likelihood of being tumor-infected victims [4]. The analysis of bone cancer is established through 3 features: Histopathologic aspect, imaging, and symptomatology. Unluckily, the signs are nonspecific, and they deliver slight information to direct the analysis to two major types of bone tumors, mainly in the initial phases of the illness [5]. The histopathologic analysis is the crucial component, which offers the utmost precise analysis and begins the therapeutic method. Assuming its aggressive nature, this analysis characterizes the concluding phase of the analytical procedure. For the highest precision, imaging information is essential to define the utmost suitable region for harvesting [6]. Because of the modern key technical improvements, imaging examinations have grown increasingly successful.

ML and AI have made rapid progress in recent times [7]. The utilization of AI and ML techniques has significantly contributed to the advancement in medical domains such as image interpretation, image registration, Image-guided therapy, medical image processing, image fusion, and image segmentation. These methods have been proven to extract and represent information from medical images in a highly effective and efficient manner. AI and ML enable and support medics so that they can analyze and forecast precise and earlier threats of illnesses and stop them [8]. These methods improve the capabilities of medics and scientists to recognize how to examine the common differences that will give rise to the illness. Though automatic recognition of illnesses depends on conservative approaches in therapeutic imaging and has been exposed to important precisions for years, novel improvements in ML methods have exploded in the DL [9]. DL-dependent procedures exhibit encouraging presentation in various fields such as drug detection, lips reading, computer-aided analysis, text identification, speech identification, lip reading, computer-aided analysis, and face identification [10].

We offer a Hybrid Rice Optimization Algorithm with DL-Assisted Bone Cancer Detection (HROADL-BCD) technique on medical X-ray images. In the presented HROADL-BCD technique, a bilateral filtering (BF) process is performed to remove the noise. To derive feature vectors, the HROADL-BCD technique applies the EfficientNet model. The HROADL-BCD technique involves the HROA for hyperparameter tuning of the EfficientNet model. Last, the bone cancer detection and classification process were applied by an attention-based bidirectional long short-term memory (ABiLSTM) system. For simulation result analysis of the HROADL-BCD algorithm, a wide range of simulations can be executed.

2. Literature review

Rehman et al. [11] designed for a tool for diagnosing osteoarthritis. The recent DL-based CNN and numerous ML-based algorithms have been implemented for evaluation. A new TL-based feature engineering method CRK (CNN, RF, and KNN) was developed. By employing a 2D-CNN, the CRK rapidly removes the spatial features that could be transferred to the RF and KNN methods, producing probabilistic feature sets. In [12], the Seg-Unet framework with patched and global-based techniques is introduced. This technique includes higher-risk area segmentation, cancer segmentation, and classification subdivisions for learning collective advantages between the local textures at all pixels and the global context of the whole image. The patch-based algorithm increases effectiveness in malignant tumor identification.

Bharodiya and Gonsai [13] projected an intelligent assistive method named BTDBB. This developed method takes human arm X-ray images, improves to split images into various sections depending on crop image to maintain only ROI, transforms into grayscale, performs Gaussian filtering (GF) for eliminating noise and segmentation, identification of ROI employing binary blob pattern analyses, diagnosing bone cancer, threshold, and determination of cancer size. Xu et al. [14] introduced a novel necrosis rate identification technique utilizing time series X-ray images. This presented technique employs a GAN with LSTM for producing time series X-ray images. An image-to-image transferred network was implemented to generate the major images for more data extension. This data augmentation has been referred to as a training set of 3D-CNN classification techniques.

Wani and Arora [15] projected a CNN-based technique. The TL of DL-based CNNs such as VggNet19, AlexNet, ResNet, and VggNet16 could be employed for categorizing the X-ray images. Our major aims are: To introduce a database of 381 knee x-rays pathologically confirmed by the T-scores acquired in the Quantitative Ultrasound technique, and to develop a DL algorithm employing TL for classification. Singh et al. [16] suggested an innovative method for diagnosing bone cancer that depends on classification and feature extraction employing the DL approach. After preprocessing, the features are removed by exploiting ROI extraction and Convolution HOG gradients (CHOG) technique. To classify the correct spotting and grading of the bone tissue as abnormal and normal, the presented model utilized the extreme Convolutional DL machine (ECDLM) approach.

In [17], a multi-feature aggregation block called a combined gate was presented. This developed combined gate is to make a regenerated feature, which includes both higher-level and lower-level data. Therefore, the regenerated feature was integrated with the smaller scare feature cued with a local feature fusion algorithm, attaining multi-scare feature aggregation. Moreover, an innovative X-ray image database has been developed for segmenting bone cancers. Gül et al. [18] implemented an innovative DL-based technique for automatically detecting pes planus through X-ray images. A novel

pes planus database was employed. Followed by preprocessing, the images are provided to the pre-training MobileNetV2, and features are removed in the Logits layer.

3. The proposed model

In this manuscript, an automated bone cancer detection method known as the HROADL-BCD technique on X-ray images is presented. The major intention of the HROADL-BCD technique is to inspect the X-ray images for the recognition of bone cancer. In the proposed HROADL-BCD method, dissimilar phases of operations are BF-based noise removal, EfficientNet feature extraction, ABiLSTM-based classification, and HROA-based hyperparameter tuning. Figure 1 depicts the working process of the HROADL-BCD method.

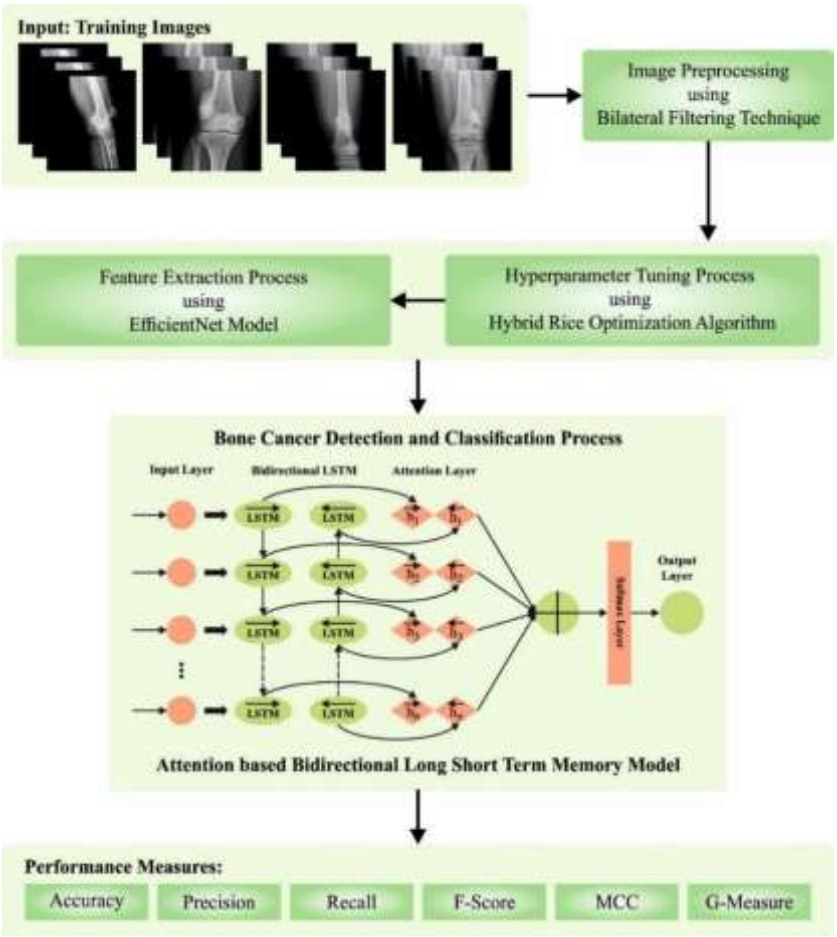

Figure 1. Overall procedure of the HROADL-BCD approach.

3.1. Image preprocessing

The BF approach is used to eliminate the noise in the X-ray images. In X-ray imaging, noise, including speckle and Gaussian noise, poses a crucial threat, complicating critical anatomical details and hindering precise diagnosis. Hence, the BF model is significant in mitigating these problems, selectively mitigating noise while safeguarding needful image features and sharp transitions. BF is a

great image processing system to efficiently improve and denoise images by maintaining boundaries and fine parts [19]. It accomplishes this by assuming either spatial proximity pixel intensity or color similarity once executing a weighted average filtering to adjacent pixels. This method permits BF for smoothing areas with the same preserving sharp transitions, making it a useful tool in distinct image processing applications comprising tone mapping, edge-preserving smoothing, and image denoising, but preserving image fidelity and infrastructure is essential for high-quality performances.

3.2. Feature extraction

To generate features, the EfficientNet model is applied. EfficientNet is a ground-breaking family of CNN designs, which has caused a major control on the domain of computer vision (CV) [20]. Established by Google's researchers, EfficientNet is known for accomplishing an impressive balance between computational performance and accuracy, making it extremely sought-after for extracting features in distinct image processing and CV tasks. At the center, EfficientNet establishes a new method for scaling the model design, suggested as compound scaling. This method entails scaling the width, resolution, and depth of NN. As a result, EfficientNet optimizes its solution, making sure that as the model dimension enhances, its capability to capture intricate designs and representations is also enhanced. This outcome in methods could not only be extremely effectual but also remarkably correct, making it ideal for extracting features from the application ranges. The compound scaling in EfficientNet is directed by a scaling coefficient, signified as "phi" (ϕ), which handles the model's dimensional and capacity. As ϕ enhances, the model becomes greater and more important. Figure 2 portrays the infrastructure of EfficientNet.

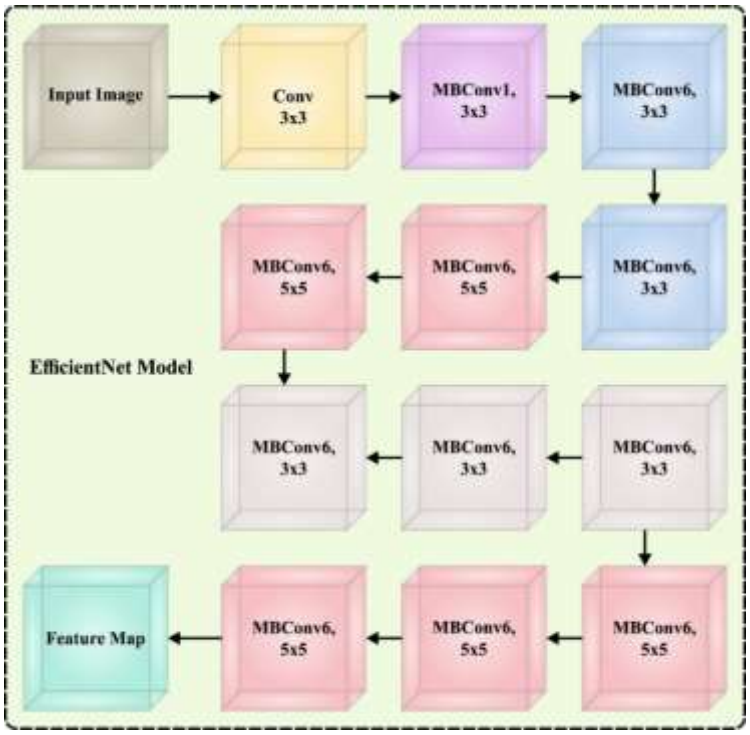

Figure 2. Architecture of EfficientNet.

The EfficientNet base structure, called EfficientNetB0, was planned with a certain balance of depth, width (i.e., the count of channels from all the layers), and image resolution. It further involves the MobileNetV2 structure that is recognized for its lightweight design, creating it an effective optimal for computation. EfficientNet establishes scaling factors for depth, width, and resolution, expressed as α, β, and γ, correspondingly. These factors define that several dimensions of networks can be scaled once ϕ is enhanced. This scaling approach makes sure that higher methods preserve similar comparative proportions as their lesser counterparts, maintaining structural integrity. EfficientNet provides a range of model variations, implied as B0-B7, with a distinct ϕ value. The B0 difference is the minimum and more computationally effective, but B7 is the maximum and most important. This scalability permits practitioners to select the model differently to be suited for its computational resources and performance requirements. Lesser variants are ideal for utilization in resource-constrained environments, but higher variants offer existing solutions for an extensive array of image detection tasks.

3.3. Hyperparameter tuning

In this work, the HROA was executed for the hyperparameter selection of the EfficientNet model. Ye et al. proposed that HRO is a state-of-the-art metaheuristic approach stimulated by the advantages of heterosis, which offers robust global search capabilities and superior search efficiency [21]. Based on their fitness values, HRO splits the population into three lines. Consider $X = (X_1, X_2, \dots, X_n)$ as the population is arranged by fitness value, but the population size is represented as n. The initial sub-population defined by $X_1, X_2, \dots, X_p (p = \lfloor n/3 \rfloor)$ possesses the best fitness, and constitutes a maintainer line. The second sub-population denoting the poor fitness value from the population is known as the sterile line and it is indicated as $X_{2p+1}, X_{2p+2}, \dots, X_n$, which needs hybridization with the maintainer line to better their fitness quality. The restorer line is the residual sub-population, represented by $X_{p+1}, X_{p+2}, \dots, X_{2p}$. Through the selfing process, it evolves into the maintainer line. In the following section, the basic principles of HRO are further discussed.

The hybridization procedure includes crossing the maintainer and sterile lines that possess major differences in their fitness values. By replacing original individuals with new hybrid individuals, the sterile line can be updated if it shows better fitness. Using Eq. (1), the newly generated individuals within the sterile line can be attained:

$$\begin{cases} X_{new(i)}^{d}(t) = r_1 \cdot X_s^d(t) + (l - r_1) \cdot X_m^d(t) \\ m \in \{1,2, \dots, p\}; i, s \in \{2p + 1, 2p + 2, n\} \end{cases} \tag{1}$$

where $X_s^d(t)$ and $X_m^d(t)$ are the d_{th} genes of random individuals chosen from the sterile and maintainer lines. r_1 is a random integer within the interval of [0,1]. $X_{new(i)}^{d}(t)$ refers to the d_{th} gene of i_{th} hybrid individuals of the sterile line at t_{th} iterations.

Selfing

This process is used for updating the restorer line, to steer the individuals toward the best global solution. Such behaviors are mathematically modeled as follows:

$$\begin{cases} X_{new(i)}^{d}(t) = r_2\left(X_{best}^{d}(t) - X_{r(j)}^{d}(t)\right) + X_{r_{(i)}}^{d}(t), \\ i, j \in \{p+1, p+2, .., 2p\}, j \neq i, \end{cases} \tag{2}$$

In Eq (2), $(j \neq i)$, a new gene generated by selfing between i_{th} and j_{th} restorer is $X_{new(i)}^{d}(t)$. $X_{r(j)}^{d}(t)$ signifies the d_{th} gene of the restorer selected arbitrarily in the restorer line and $X_{best}^{d}(t)$ denotes the d_{th} gene of the best individual obtained. The parameter r_2 is a randomly generated number from [0,1].

The original candidate solution was evaluated and compared after the generation of the newest individual through hybridization and selfing. As defined in Eq (3), the substitution process is used to replace the old individuals with newer ones as long as the fitness values of a new individual exceed the old one.

$$X_i(t+1) = \begin{cases} X_{new(i)}(t), & iff\left(X_{new(i)}(t)\right) > f\left(X_i(t)\right), \\ X_i(t), & otherwise. \end{cases} \tag{3}$$

The selfing procedure in HRO includes tracking the iteration number while the restorer cannot endure upgrades utilizing self-crossing parameters (SC). When the restorer's SC obtains the upper boundary, represented as $t_{\max}$ iteration without upgrades, then the reset operation can be implemented for that individual. The mathematical modeling of a reset behavior is given below:

$$X_{r(i)}^{d}(t+1) = r_3\left(V_{\max}^{d} - V_{\min}^{d}\right) + X_{r(i)}^{d}(t) + V_{\min}^{d}, \tag{4}$$

In Eq (4), $X_{r(i)}^{d}(t)$ shows that the d_{th} gene of i_{th} restorer that has not been upgraded, and the maximal and minimal values of d_{th} dimension are $V_{\max}^{d}$ and $V_{\min}^{d}$ correspondingly. r_3 refers to the random value ranging from zero and one. Note that the performance attained by HRO is continuous and should be mapped into the solution space of FS using the transfer function applications. The sigmoid function is used as a binary map that can be described as follows:

$$sigmoid\ (x) = \frac{1}{1+e^{-x}}, \tag{5}$$

$$X_i^d = \begin{cases} 1, & if\ sigmoid\left(X_i^d\right) > rand, \\ 0, & otherwise, \end{cases} \tag{6}$$

The HRO algorithm progresses a fitness function (FF) to achieve an enhanced classifier solution. It is used to express the positive integer to state the good efficiency of candidate performance. Here, the decreasing classifier errors are assumed as FF, as depicted in Eq (7).

$$\begin{aligned} fitness(x_i) &= ClassifierErrorRate(x_i) \\ &= \frac{No.of\ misclassified\ samples}{Total\ No.of\ samples} * 100 \end{aligned} \tag{7}$$

3.4. Image classification

The HROADL-BCD model has been applied to the ABiLSTM model for the image classification

process. The LSTM-NN is developed, which relies on RNN for resolving the disappearing and explosion gradient problems [22]. LSTM could capture the standard features of the input dataset. The above problems are efficiently evaded as a parameter of each structure as independent. The internal structure of LSTM is made up of a memory cell c_t, an input gate i_t, forget gate f_t, output gate 0_t, and existing output h_t. The output values of prior unit h_{t-1}, the cell layer of prior unit c_{t-1}, and the input database x_i are exploited as input for existing units. Using the following formula, LSTM is defined:

$$f_t = \sigma\left(W_f x_t + U_f h_{t-1} + b_f\right) \tag{8}$$

$$i_t = \sigma(W_i x_t + U_i h_{t-1} + b_i) \tag{9}$$

$$O_t = \sigma(W_o x_t + U_o h_{t-1} + b_o) \tag{10}$$

$$\tilde{c}_t = \tanh(W_c x_t + U_c h_{t-1} + b_c) \tag{11}$$

$$c_t = f_t \odot c_{t-1} + i_t \odot \tilde{c}_t \tag{12}$$

$$h_t = O_t \odot \tanh(C) \tag{13}$$

where $\odot$ indicates the Hadamard product, W_f, U_f, W_i, U_i, W_o, U_o, W_c, and U_c are the weighted matrices, b_f, b_i, b_o, and b_c are bias vectors, and σ and tanh denote the activation functions. The formula is given below:

$$\sigma(x) = \frac{1}{1 + e^x} \tag{14}$$

$$\tanh(x) = \frac{e^x - e^{-x}}{e^x + e^{-x}} \tag{15}$$

$$\hat{y}_{t+1} = \tanh\left(h_t W_y + b_y\right) \tag{16}$$

In Eq (16), b_y is the bias vector, and W_y is the weight matrix.

Accordingly, Graves and Schmidhuber introduced Bi-LSTM that fuses forward and reverse LSTM. It has more benefits in terms of prediction since it extracts time series data. x is provided as the reverse and forward LSTM to attain the output of LSTM. The predicted values can be evaluated by Eq (17):

$$\hat{y}_{t+1} = \tanh\left(\vec{h}_t W_y + \overleftarrow{h}_t U_y + b_y\right) \tag{17}$$

here, $\vec{h}_t$ and $\overleftarrow{h}_t$ imply the output results of forward as well as reverse LSTM. W_y and U_y denote the weighted matrices and b_y is a bias vector.

There are some differences in the importance of time series features. Based on the CNN and BiLSTM, we present an attention model for assigning weight to the element in the feature sequence. The attention model highlights relevant features, decreases the impact of weakly related features, and assists the model in making more accurate evaluations as follows:

$$Att = \sum_{i=1}^{m} soft\,max\left(f(x_i)\right) * x_i \tag{18}$$

In Eq (18), the feature sequence input to the layer of the attention module is x_i, and the weighted sum of weight.

4. Results and discussion

In this study, the experimental outcome of the HROADL-BCD approach is tested on a dataset [23], including 200 samples and 2 classes as denoted in Table 1.

Table 1. Details on database.

Class Name	No. of Instances
Cancerous	100
Healthy	100
Total No. of Instances	200

The confusion matrices offered by the HROADL-BCD technique on 70:30 and 80:20 of the TRPH/TSPH are illustrated in Figure 3. The outcome indicates the effective recognition of the healthy and cancerous samples under each 2 class labels.

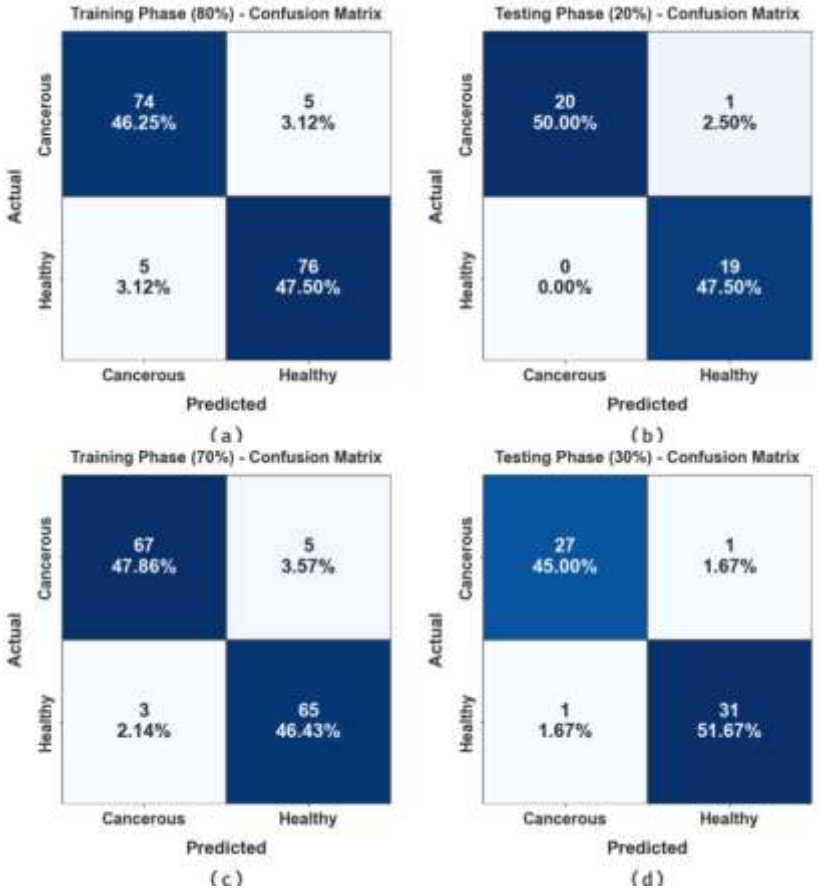

Figure 3. Confusion matrices of (a-c) TR phase (TRPH) of 80% and 70%, and (b-d) TS phase (TSPH) of 20% and 30%.

The bone cancer detection outcomes of the HROADL-BCD technique are examined on 80:20 of the TRPH/TSPH as shown in Table 2 and Figure 4. The simulated outcomes pointed out that the HROADL-BCD method proficiently classifies every 2 samples. Moreover, based on 80% of the TRPH, the HROADL-BCD technique obtains average $accu_y$, $Prec_n$, $Reca_l$, F_{score}, MCC, and $G-Measure$ values of 93.75%, 93.75%, 93.75%, 93.75%, 87.50%, and 93.75% respectively. Likewise, with 20% of the TSPH, the HROADL-BCD system attains average $accu_y$, $Prec_n$, $Reca_l$, F_{score}, MCC, and $G-Measure$ values of 97.62%, 97.50%, 97.62%, 97.50%, 95.12%, and 97.53%, respectively.

Table 2. Bone cancer detection outcome of the HROADL-BCD method on 80:20 of TRPH/TSPH.

Class	$Accu_y$	$Prec_n$	$Reca_l$	F_{score}	MCC	G-Measure
TRPH (80%)						
Cancerous	93.67	93.67	93.67	93.67	87.50	93.67
Healthy	93.83	93.83	93.83	93.83	87.50	93.83
Average	93.75	93.75	93.75	93.75	87.50	93.75
TSPH (20%)						
Cancerous	95.24	100.00	95.24	97.56	95.12	97.59
Healthy	100.00	95.00	100.00	97.44	95.12	97.47
Average	97.62	97.50	97.62	97.50	95.12	97.53

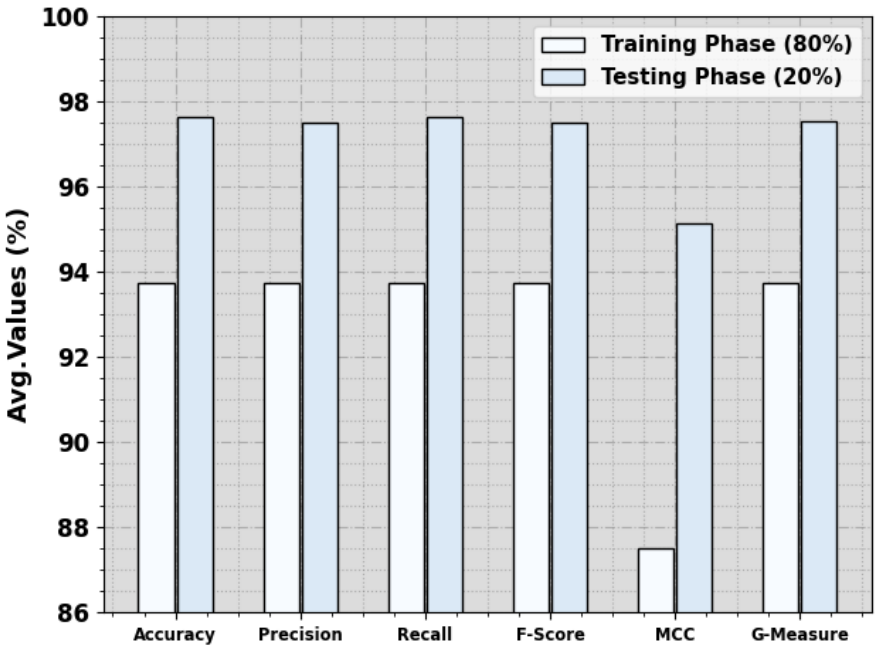

Figure 4. Average of the HROADL-BCD method on 80:20 of TRPH/TSPH.

The bone cancer detection examination of the HROADL-BCD method can be investigated at 70:30 of the TRPH/TSPH as shown in Table 3 and Figure 5. The simulated outcomes denote that the HROADL-BCD system categorizes 2 samples efficiently.

Table 3. Bone cancer detection outcome of HROADL-BCD method at 70:30 of TRPH/TSPH.

Class	$Accu_y$	$Prec_n$	$Reca_l$	F_{score}	MCC	G-Measure
TRPH (70%)						
Cancerous	93.06	95.71	93.06	94.37	88.61	94.38
Healthy	95.59	92.86	95.59	94.20	88.61	94.21
Average	94.32	94.29	94.32	94.28	88.61	94.29
TSPH (30%)						
Cancerous	96.43	96.43	96.43	96.43	93.30	96.43
Healthy	96.88	96.88	96.88	96.88	93.30	96.88
Average	96.65	96.65	96.65	96.65	93.30	96.65

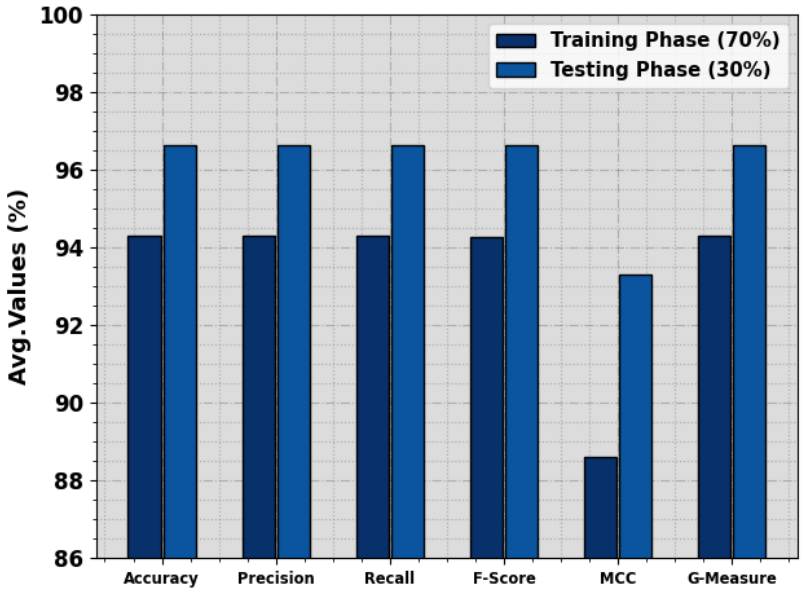

Figure 5. Average of the HROADL-BCD method at 70:30 of TRPH/TSPH.

Based on 70% of the TRPH, the HROADL-BCD technique gets average $accu_y$, $Prec_n$, $Reca_l$, F_{score}, MCC, and $G-Measure$ values of 94.32%, 94.29%, 94.32%, 94.28%, 88.61%, and 94.29%, respectively. Based on 30% of TSPH, the HROADL-BCD system obtains average $accu_y$, $Prec_n$, $Reca_l$, F_{score}, MCC, and $G-Measure$ values of 96.65%, 96.65%, 96.65%, 96.65%, 93.30%, and 96.65% respectively.

To calculate the performance of the HROADL-BCD methodology on 80:20 of TRPH/TSPH, TR, and TS $accu_y$ curves are shown in Figure 6. The TR and TS $accu_y$ curves demonstrate the outcome of the HROADL-BCD method over several epochs. The figure offers related details regarding the learning task and generalizability of the HROADL-BCD system. The TR and TS $accu_y$ curves are enhanced with increasing epoch count. The HROADL-BCD approach gets enriched TS accuracy that can identify the patterns in the TR and TS datasets.

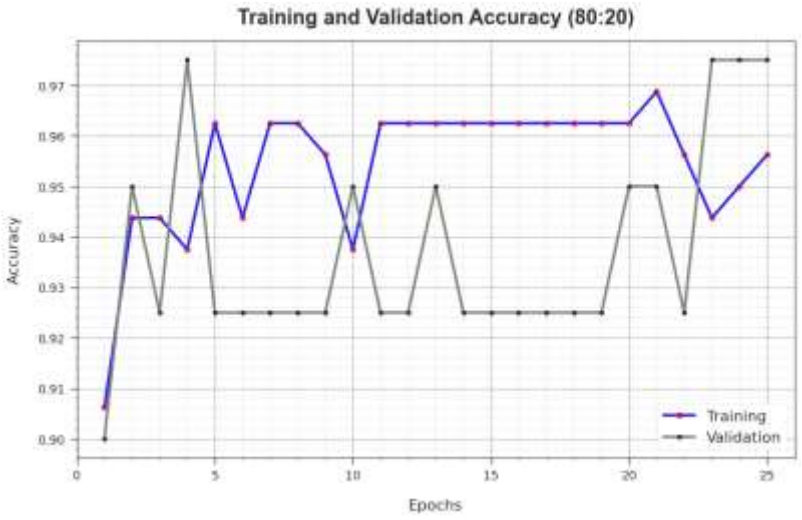

Figure 6. $Accu_y$ curve of HROADL-BCD method on 80:20 of TRPH/TSPH.

The TR and TS loss values of the HROADL-BCD system on 80:20 of TRPH/TSPH over epochs are illustrated in Figure 7. The TR loss depicts that the model loss attained decreased over epochs. The loss value attained was minimized as the model adapted the weight for diminishing the prediction errors for the TR and TS datasets. The loss analysis denotes how well the model fits the TR dataset. TR and TS loss is gradually minimized and defined so that the HROADL-BCD system learns the pattern exposed in the TR and TS data. The HROADL-BCD method adapts the parameter to reduce the variation between the training labels and predictions.

The PR performance of the HROADL-BCD system on 80:20 of TRPH/TSPH is demonstrated by plotting precision against recall as described in Figure 8. The outcome inferred that the HROADL-BCD method obtains high PR values under 2 classes. The result demonstrates that the model identifies different classes. The HROADL-BCD obtains high efficiency in detecting positive instances with reduced false positives.

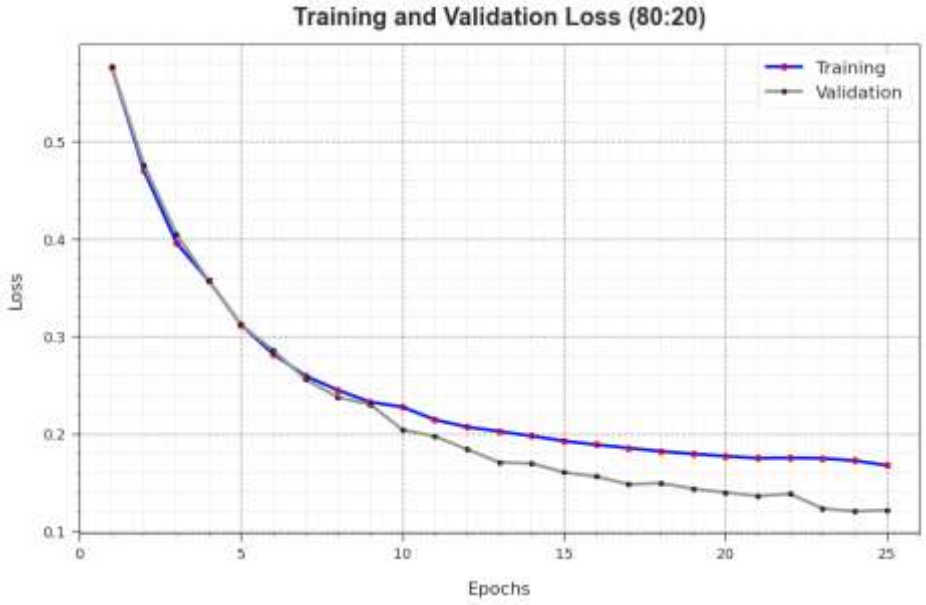

Figure 7. Loss curve of the HROADL-BCD method at 80:20 of TRPH/TSPH.

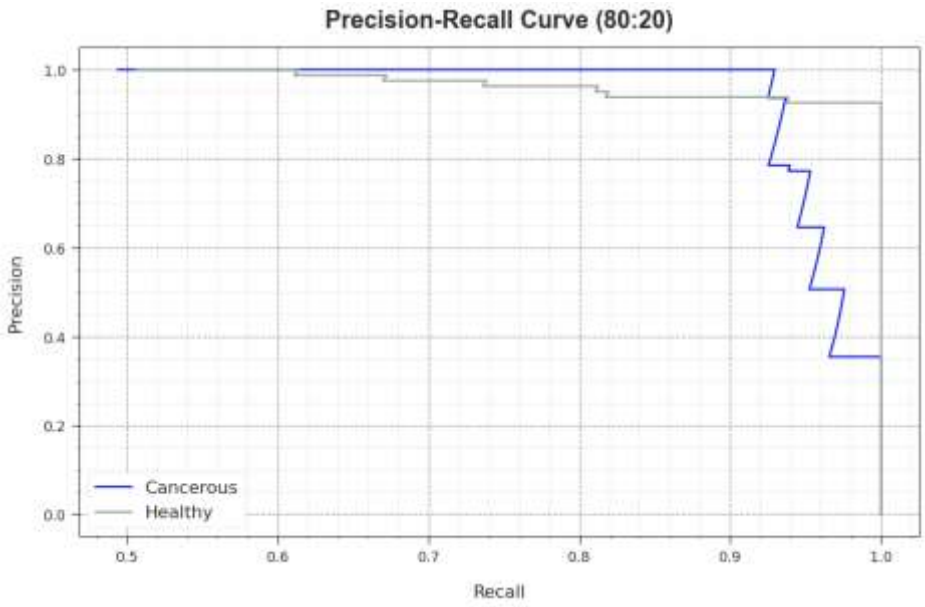

Figure 8. PR curve of the HROADL-BCD method on 80:20 of TRPH/TSPH.

The ROC examination offered by the HROADL-BCD method on 80:20 of TRPH/TSPH is depicted in Figure 9. The outcome shows valuable insights into the tradeoffs between TPR and FPR rates with divergent classifier thresholds and dissimilar epoch count. It presents the correct predicted solution of the HROADL-BCD method for the classifier of 2 classes.

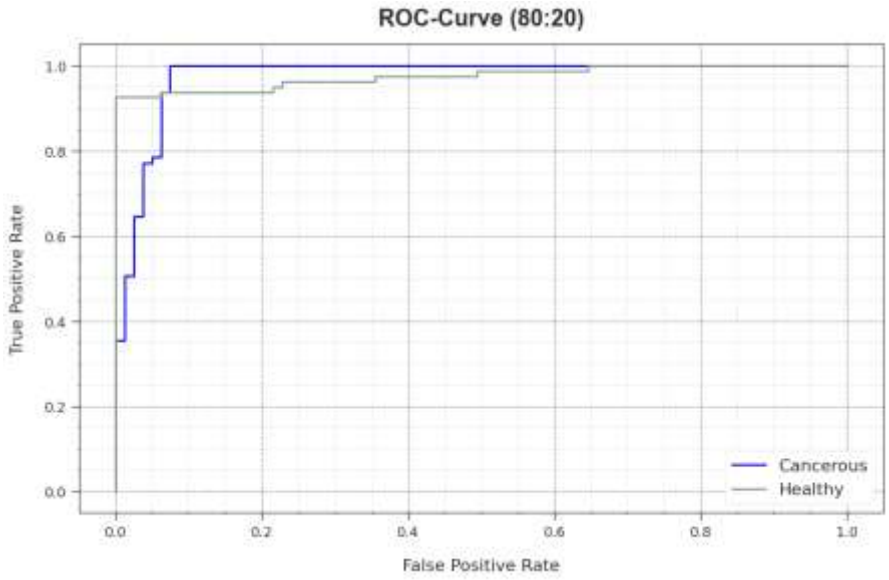

Figure 9. ROC curve of HROADL-BCD method at 80:20 of TRPH/TSPH.

The cancer detection performance of the HROADL-BCD technique is compared with recent techniques in Table 4 and Figure 10. The simulated values exhibit that the RF, ResNet50, and Inceptionv3 algorithms obtained poorer performance while the SVM, BCDFE-ML, and Efficient-Net systems obtained moderately enhanced results.

Table 4. Comparative outcome of the HROADL-BCD method with other systems.

Methods	$Accu_y$	$Prec_n$	$Reca_l$	F_{score}
HROADL-BCD	97.62	97.50	97.62	97.50
OSADL-BCDC	95.00	95.02	95.00	95.00
RF	69.05	75.69	79.07	77.71
SVM	92.59	90.63	93.58	93.13
BCDFE-ML	92.48	92.70	89.17	93.83
ResNet50	82.57	81.02	78.92	81.75
InceptionV3	83.33	81.48	89.74	78.10
Efficient-Net	85.79	82.28	91.53	83.61

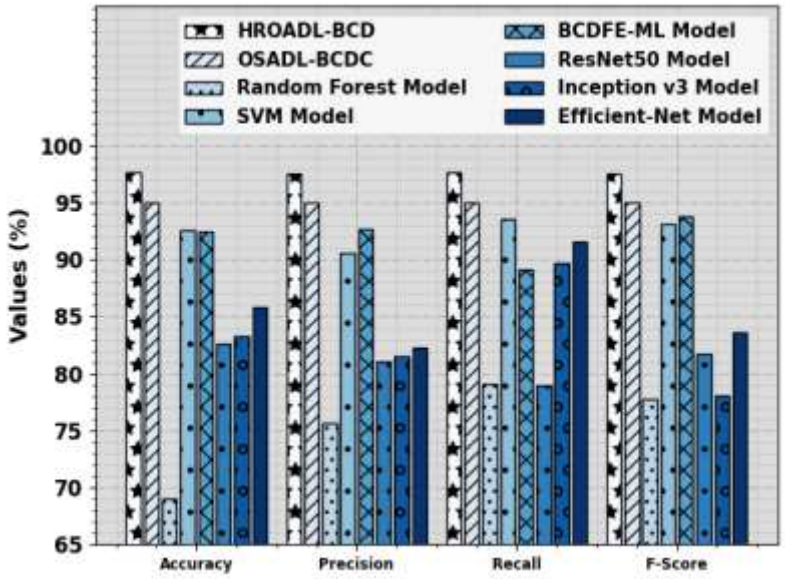

Figure 10. Comparative outcome of the HROADL-BCD method with other techniques.

The OSADL-BCDC model has shown considerable outcomes. However, the HROADL-BCD technique achieves better results with raised $accu_y$, $prec_n$, $reca_l$, and F_{score} of 97.62%, 97.50%, 97.62%, and 97.50%, respectively. Therefore, the HROADL-BCD technique exhibits optimal performance in the bone cancer detection and classification process.

5. Conclusions

In this manuscript, an automated bone cancer detection method called the HROADL-BCD technique on X-ray images is presented. The major aim of the HROADL-BCD technique is to inspect the X-ray images for bone cancer detection. In the presented HROADL-BCD method, dissimilar phases of operations are BF-based noise removal, EfficientNet feature extraction, HROA-based tuning, and ABiLSTM-based classification. For hyperparameter tuning of the EfficientNet model, the HROADL-BCD technique uses the HROA. The bone cancer detection and classification process are performed using the ABiLSTM model. For experimental result analysis of the HROADL-BCD system, a wide range of simulations is executed. The extensive outcome inferred the improved outcome of the

HROADL-BCD approach concerning various aspects.

Use of AI tools declaration

The authors declare that they have not used Artificial Intelligence (AI) tools in the creation of this article.

Acknowledgments

The authors extend their appreciation to the Deputyship for Research and Innovation, Ministry of Education in Saudi Arabia for funding this research work through the project number (IF2/PSAU/2022/01/23005).

Conflict of interest

The authors declare that they have no conflicts of interest.

Author contributions

T.V.: Conceptualization; P.B.: Data curation; P.B.: Formal analysis; S.S.: Investigation; T.V. and S.S.: Methodology; N.A. and S.M.: Validation; A.M.: Visualization; T.V.: Writing—original draft; P.B.; Writing—review & editing. All authors have read and agreed to the published version of the manuscript.

References

1. S. Breden, F. Hinterwimmer, S. Consalvo, J. Neumann, C. Knebel, R. Eisenhart-Rothe, et al., Deep learning-based detection of bone tumors around the Knee in X-rays of children, *J. Clin. Med.,* **12** (2023), 1–9.
2. K. Furuo, K. Morita, T. Hagi, T. Nakamura, T. Wakabayashi, Automatic benign and malignant estimation of bone tumors using deep learning, *2021 5th IEEE International Conference on Cybernetics (CYBCONF)*, Sendai, Japan, 2021, 030–033, https://doi.org/10.1109/CYBCONF51991.2021.9464132
3. M. H. Mazumder, M. P. Singh, Bone cancer detection using deep learning. *In International Conference on Innovations in Computer Science and Engineering*, 285–296, 2022. Singapore: Springer Nature Singapore.
4. B. S. Vandana, S. R. Alva, Deep Learning Based Automated tool for cancer diagnosis from bone histopathology images, *2021 International Conference on Intelligent Technologies (CONIT)*, Hubli, India, 2021, 1–8. https://doi.org/10.1109/CONIT51480.2021.9498367
5. A. Shukla, A. Patel, Bone cancer detection from X-ray and MRI images through image segmentation techniques, *Int. J. Recent Technol. Eng.,* **8** (2020), 273–278.
6. S. Gawade, A. Bhansali, K. Patil, D. Shaikh, Application of the convolutional neural networks and supervised deep-learning methods for osteosarcoma bone cancer detection, *Health. Anal.,* **3** (2023), 100153.

7. T. Zimbalist, R. Rosen, K. Peri-Hanania, Y. Caspi, B. Rinott, Detecting bone lesions in X-Ray under diverse acquisition conditions, arXiv preprint arXiv:2212.07792., 2022. https://doi.org/10.1117/1.JMI.11.2.024502
8. H. X. Huynh, H. B. T. Nguyen, C. A. Phan, H. T. Nguyen, Abnormality Bone Detection in X-Ray Images Using Convolutional Neural Network, *In Context-Aware Systems and Applications, and Nature of Computation and Communication: 9th EAI International Conference, ICCASA 2020, and 6th EAI International Conference, ICTCC 2020,* Thai Nguyen, Vietnam, Proceedings 9, 31–43, 2021. Springer International Publishing.
9. G. Suganeshwari, R. Balakumar, K. Karuppanan, S. B. Prathiba, S. Anbalagan, DTBV: A deep transfer-based bone cancer diagnosis system using VGG16 feature extraction, *Diagnostics,* 13 (2023), 757.
10. F. R. Eweje, B. Bao, J. Wu, D. Dalal, W. H. Liao, Y. He, et al., Deep learning for classification of bone lesions on routine MRI, *EBioMedicine,* 68*,* 2021. https://doi.org/10.1016/j.ebiom.2021.103402
11. A. Rehman, A. Raza, F. S. Alamri, B. Alghofaily, T. Saba, Transfer learning-based smart features engineering for osteoarthritis diagnosis from knee X-Ray images, *IEEE Access*, **11** (2023), 71326–71338, 2023. https://doi.org/10.1109/ACCESS.2023.3294542
12. N. T. Do, S. T. Jung, H. J. Yang, S. H. Kim, Multi-level seg-unet model with global and patch-based X-ray images for knee bone tumor detection, *Diagnostics,* **11** (2021), 691.
13. A. K. Bharodiya, A. M. Gonsai, An intelligent assistive algorithm for bone tumor detection from human X-ray images based on binary Blob analysis, *Int. J. Inf. Technol.,* 1–7, 2020. https://doi.org/10.1007/s41870-020-00539-0
14. Z. Xu, K. Niu, S. Tang, T. Song, Y. Rong, W. Guo, et al., Bone tumor necrosis rate detection in few-shot X-rays based on deep learning, *Comput. Med. Imag. Grap.,* **102** (2022), 102141.
15. I. M. Wani, S. Arora, Osteoporosis diagnosis in knee X-rays by transfer learning based on convolution neural network, *Multimed. Tools Appl.,* **82** (2023), 14193–14217.
16. M. Singh, M. Angurala, M. Bala, Bone tumour detection using feature extraction with classification by deep learning techniques, *Res. J. Comput. Syst. Eng.,* **1** (2020), 23–27.
17. Z. Xie, K. Zhao, X. Yan, S. Wu, J. Mei, H. Lu, Merged U-Net for Bone Tumors X-Ray Images Segmentation, *2022 IEEE International Conference on Image Processing (ICIP)*, Bordeaux, France, 2022. 1276–1280. https://doi.org/10.1109/ICIP46576.2022.9897539
18. Y. Gül, S. Yaman, D. Avcı, A. H. Çilengir, M. Balaban, H. Güler, A novel deep transfer learning-based approach for automated Pes Planus diagnosis using X-ray image, *Diagnostics,* **13** (2023), 1662.
19. H. Li, X. L. Duan, SAR Ship Image Speckle Noise Suppression Algorithm based on adaptive bilateral filter, *Wirel. Commun. Mob. Comput.,* 2022. https://doi.org/10.1155/2022/9392648
20. K. Yousaf, T. Nawaz, A. Habib, Using two-stream EfficientNet-BiLSTM network for multiclass classification of disturbing YouTube videos, *Multimed. Tools Appl.,* 1–28, 2023. https://doi.org/10.1007/s11042-023-15774-3
21. A. Z. Ye, B. R. Li, C. W. Zhou, D. M. Wang, E. M. Mei, F. Shu, et al., High-Dimensional feature selection based on improved Binary Ant Colony Optimization combined with Hybrid Rice Optimization Algorithm, *Int. J. Intell. Syst.,* 2023. https://doi.org/10.1155/2023/1444938
22. W. Zeng, K. Wang, J. Zhou, R. Cheng, Traffic Flow Prediction based on hybrid deep learning models considering missing data and multiple factors, *Sustainability,* **15** (2023), 11092.

23. E. Alabdulkreem, M. K. Saeed, S. S. Alotaibi, R. Allafi, A. Mohamed, M. A. Hamza, Bone cancer detection and Classification Using Owl Search Algorithm with deep learning on X-Ray images, *IEEE Access*, 11 (2023), 109095–109103. https://doi.org/10.1109/ACCESS.2023.3319293

AIMS Press